

## Article

# Differences in Secondary Organic Aerosol Formation from $\alpha$ -Pinene Photooxidation in a Chamber with Purified Air and Ambient Air as Matrices: Preliminary Results

Xinyi Li <sup>1,2</sup>, Zhuoyue Ren <sup>1,2</sup>, Xiangyu Zhang <sup>1,2</sup>, Xiaodie Pang <sup>1,2</sup>, Wei Song <sup>1</sup>, Yanli Zhang <sup>1,2</sup> and Xinming Wang <sup>1,2,\*</sup> 

<sup>1</sup> State Key Laboratory of Organic Geochemistry, Guangdong Key Laboratory of Environmental Protection and Resources Utilization, Guangzhou Institute of Geochemistry, Chinese Academy of Sciences, Guangzhou 510640, China

<sup>2</sup> University of Chinese Academy of Sciences, Beijing 100049, China

\* Correspondence: wangxm@gig.ac.cn

**Abstract:**  $\alpha$ -Pinene is a biogenic volatile organic compound (BVOC) that significantly contributes to secondary organic aerosols (SOA) in the atmosphere due to its high emission rate, reactivity, and SOA yield. However, the SOA yield measured in chamber studies from  $\alpha$ -pinene photooxidation is limited in a purified air matrix. Assessing SOA formation from  $\alpha$ -pinene photooxidation in real urban ambient air based on studies conducted in purified air matrices may be subject to uncertainties. In this study,  $\alpha$ -pinene photooxidation and SOA yield were investigated in a smog chamber in the presence of NO and SO<sub>2</sub> under purified air and ambient air matrices. With the accumulation of ozone (O<sub>3</sub>) during the photooxidation, an increasing part of  $\alpha$ -pinene was consumed by O<sub>3</sub> and finally nearly half of the  $\alpha$ -pinene was oxidized by O<sub>3</sub>, facilitating the production of highly oxidized organic molecules and thereby SOA formation. Although the ambient air we introduced as matrix air was largely clean, with initial organic aerosol mass concentrations of  $\sim 1.5 \mu\text{g m}^{-3}$ , the  $\alpha$ -pinene SOA yield in the ambient air matrix was  $42.3 \pm 5.3\%$ , still higher than that of  $32.4 \pm 0.4\%$  in the purified air matrix. The chemical characterization of SOA by the high-resolution time-of-flight aerosol mass spectrometer (HR-ToF-AMS) revealed that C<sub>x</sub>H<sub>y</sub> accounted for  $53.7 \pm 1.1\%$  of the total signal in the ambient air matrix experiments, higher than  $48.1 \pm 0.3\%$  in the purified air, while C<sub>x</sub>H<sub>y</sub>O and C<sub>x</sub>H<sub>y</sub>O<sub>>1</sub> together constituted  $45.0 \pm 0.9\%$  in the ambient air matrix, lower than  $50.1 \pm 1.0\%$  in the purified air. The O:C ratio in the ambient air matrix experiments was  $0.41 \pm 0.01$ , lower than  $0.46 \pm 0.01$  in the purified air. The higher SOA yield of  $\alpha$ -pinene in the ambient air matrix compared to that in the purified air matrix was partly due to the presence of initial aerosols in the ambient air, which facilitated the low volatile organic compounds produced from photochemical oxidation to enter the aerosol phase through gas-particle partitioning. The in-situ aerosol acidity calculated by the ISORROPIA-II model in the ambient air matrix experiments was approximately six times higher than that in purified air, and the higher SOA yield in the ambient air matrix experiments might also be attributed to acid-catalyzed SOA formation.

**Keywords:** secondary organic aerosols;  $\alpha$ -pinene; chamber simulation; purified air; ambient air



**Citation:** Li, X.; Ren, Z.; Zhang, X.; Pang, X.; Song, W.; Zhang, Y.; Wang, X. Differences in Secondary Organic Aerosol Formation from  $\alpha$ -Pinene Photooxidation in a Chamber with Purified Air and Ambient Air as Matrices: Preliminary Results. *Atmosphere* **2024**, *15*, 204. <https://doi.org/10.3390/atmos15020204>

Academic Editor: Mark C. Green

Received: 12 January 2024

Revised: 30 January 2024

Accepted: 3 February 2024

Published: 6 February 2024



**Copyright:** © 2024 by the authors. Licensee MDPI, Basel, Switzerland. This article is an open access article distributed under the terms and conditions of the Creative Commons Attribution (CC BY) license (<https://creativecommons.org/licenses/by/4.0/>).

## 1. Introduction

Secondary organic aerosols (SOA) are a crucial component of atmospheric aerosols, impacting human health, air quality, and climate [1,2]. The largest source of SOA in the atmosphere is the photooxidation of biogenic volatile organic compounds (BVOCs) [3,4]. Monoterpenes are the second most abundant class of BVOCs after isoprene [5]. Monoterpenes-SOA can account for half of the total SOA formed by BVOCs [6,7] and more than 20% of the global total SOA [8,9]. A previous study reported that  $\alpha$ -pinene has the highest emissions among the monoterpenes, with an annual global emission of  $27.2 \text{ Tg y}^{-1}$  [10]. To assess the contribution of  $\alpha$ -pinene to SOA formation, numerous laboratory experiments have been

conducted on  $\alpha$ -pinene photooxidation [11–15].  $\alpha$ -Pinene can react with oxidants such as hydroxyl radicals (OH), nitrate radicals ( $\text{NO}_3$ ), and ozone ( $\text{O}_3$ ) in the atmosphere to form low molecular weight carbonyls, such as alcohols and carboxylic acids, as well as high molecular weight dimers and other oxidation products, which are essential contributors to nucleation and SOA formation [13–15].

Previous studies have demonstrated that the formation of SOA from the photooxidation of  $\alpha$ -pinene is influenced by temperature, relative humidity (RH), seed aerosols, nitrogen oxides ( $\text{NO}_x$ ), and sulfur dioxide ( $\text{SO}_2$ ) [15–17].  $\text{NO}_x$  and  $\text{SO}_2$  are prevalent anthropogenic pollutants in the atmosphere. In regions with high levels of BVOC emissions, BVOC oxidation might be affected by  $\text{NO}_x$  and  $\text{SO}_2$ , which interfere with SOA formation [18].  $\text{NO}_x$  changes the fate of the  $\text{RO}_2$  radical formed during  $\alpha$ -pinene oxidation, inhibits the formation of low volatile organic compounds such as dimers, and promotes the formation of high volatile products, affecting SOA formation [15,19,20].  $\text{SO}_2$  could be oxidized to sulfuric acid, which promotes SOA formation through acid catalysis [21]. New particle formation and gas-particle partitioning could be promoted by  $\text{SO}_2$ , promoting SOA formation [20]. Sulfuric acid and sulfate could be also formed from  $\text{SO}_2$ , affecting the uptake of precursors or the reaction pathway, affecting the oxidation products of  $\alpha$ -pinene [22]. Currently, chamber studies of  $\alpha$ -pinene photooxidation and SOA formation are limited to purified air matrices [15,20,22–25]. A previous chamber study has revealed that SOA yields from the photooxidation of toluene in an ambient air matrix were much greater than those in a purified air matrix [26]. Therefore, investigating the yields and chemical compositions of SOA produced from  $\alpha$ -pinene photooxidation in an ambient air matrix compared to that in purified air could better our understanding of  $\alpha$ -pinene photooxidation mechanisms and our estimation of its SOA production in real-world atmospheric environments.

In this study, photooxidation experiments were conducted in a large indoor smog chamber on the  $\alpha$ -pinene +  $\text{NO}$  +  $\text{SO}_2$  combination using purified air and ambient air as matrices. The purposes are: (1) to investigate the matrix effects on the SOA formation from  $\alpha$ -pinene photooxidation; (2) to study and compare the chemical and physical evolutions of  $\alpha$ -pinene-derived SOA in the purified air and ambient air matrices.

## 2. Materials and Methods

### 2.1. Experiments

The experiments were conducted in the smog chamber of the Guangzhou Institute of Geochemistry, Chinese Academy of Sciences (GIG-CAS). This smog chamber contains a  $30\text{ m}^3$  Teflon reactor with various online measuring instruments. The Teflon reactor is equipped with two Teflon fans to ensure uniform mixing of the substances inside the chamber during the experiment. The reactor is in a temperature- and humidity-controlled enclosure, with black lamps mainly in the 306 nm wavelength installed on both sides of the chamber to provide the light source required to generate OH radicals during the photooxidation stage. Further details on the performance and characteristics of the GIG-CAS smog chamber can be found in the previous study [27].

Before each experiment, the reactor was flushed with dry and purified air. In the purified air matrix experiments, the background of the reactor contained  $<1$  ppb  $\text{O}_3$  and  $\text{NO}_x$ , and the number concentration of particles was close to 0. Approximately  $60\ \mu\text{L}$  of  $\alpha$ -pinene (A.R., Sigma Aldrich, St. Louis, MO, USA) and approximately  $2.5\ \mu\text{L}$  of butanol-d9 (98 atom% D, Sigma Aldrich, St. Louis, MO, USA) were evaporated in the heating system and injected into the chamber with high purity nitrogen. In the photooxidation stage, the loss rate of butanol-d9 was measured online and used to calculate the OH concentration [28]. More details about the calculation of OH concentration can be found in Text S1 and Figure S1.  $\text{NO}$  and  $\text{SO}_2$  were added to the reactor from the compressed gas cylinder. Table 1 shows the initial conditions of the  $\alpha$ -pinene photooxidation experiments in purified air and in the ambient air matrix. In the purified air matrix experiments, the photooxidation reaction temperature and RH were  $25.4 \pm 0.3\ ^\circ\text{C}$  and  $46.4 \pm 2.8\%$ , respectively, and the initial concentrations of  $\alpha$ -pinene,  $\text{NO}$ , and  $\text{SO}_2$  were  $110.9 \pm 12.2$  ppb,  $53.7 \pm 1.1$  ppb,

and  $78.2 \pm 4.7$  ppb, respectively. In the ambient air matrix experiments, the temperature was  $25.2 \pm 0.5$  °C and RH was  $47.0 \pm 6.9\%$ , and the initial concentrations of  $\alpha$ -pinene, NO, and SO<sub>2</sub> were  $100.6 \pm 1.8$  ppb,  $51.9 \pm 1.9$  ppb, and  $74.5 \pm 1.7$  ppb, respectively. In the ambient air matrix experiments, the initial background aerosols concentration was  $1.3 \pm 0.2$   $\mu\text{g m}^{-3}$ , the number concentration was  $1061 \pm 339$  particles  $\text{cm}^{-3}$ , and the surface area concentration was  $42 \pm 4$   $\mu\text{m}^2 \text{cm}^{-3}$ . It is worth noting that we introduced ambient air into the chamber during a locally clean day with much lower PM<sub>2.5</sub> (particulate matter with diameters less than 2.5  $\mu\text{m}$ ) pollution, and we maintained the SO<sub>2</sub> at much higher levels ( $\sim 80$  ppb) to assure the differences arose not from the difference in SO<sub>2</sub> levels.

**Table 1.** Initial conditions and SOA yields for chamber experiments with purified air and ambient air as matrices along with the calculated OH radical concentrations ( $\times 10^6$  molecules  $\text{cm}^{-3}$ ).

	Matrix Air	T (°C)	RH (%)	[NO] <sub>0</sub> (ppb)	[NO <sub>2</sub> ] <sub>0</sub> (ppb)	[SO <sub>2</sub> ] <sub>0</sub> (ppb)	[ $\alpha$ -Pinene] <sub>0</sub> (ppb)	$\Delta$ [ $\alpha$ -Pinene] (ppb)	[O <sub>3</sub> ] <sub>max</sub> (ppb)	OH	M <sub>0</sub> ( $\mu\text{g m}^{-3}$ )	PN <sup>a</sup> ( $\text{cm}^{-3}$ )	SA <sup>b</sup> ( $\mu\text{m}^2 \text{cm}^{-3}$ )	SOA ( $\mu\text{g m}^{-3}$ )	SOA Yield (%)
Exp. 1	Purified	25.0	49.7	52.2	0.8	84.8	127.0	102.1	52.2	6.33	— <sup>c</sup>	—	—	186.6	32.9
Exp. 2		25.5	46.5	54.5	0.6	74.6	108.3	98.6	57.8	2.80	—	—	—	174.6	32.0
Exp. 3		25.7	42.9	54.4	0.7	75.2	97.5	89.2	61.6	2.44	—	—	—	159.8	32.3
Exp. 4	Ambient	25.7	56.7	54.5	23.7	76.4	103.0	96.8	64.1	3.31	1.4	686	37	190.9	35.7
Exp. 5		24.5	41.7	50.2	30.3	72.3	100.1	91.6	64.7	6.60	1.0	1508	41	221.6	43.8
Exp. 6		25.4	42.6	51.1	32.5	74.9	98.6	92.5	77.4	3.44	1.6	989	47	250.2	48.6
Exp. BK		24.4	43.9	53.4	24.0	77.8	—	—	6.4	—	1.4	836	33	2.4	—

<sup>a</sup> PN is the number concentration of initial background aerosols. <sup>b</sup> SA is the surface area concentration of initial background aerosols. <sup>c</sup> — indicates that it was not added in the experiments.

In the purified air matrix experiments, photooxidation lasted about 6 h, and it lasted about 4–5 h in the ambient air matrix experiments. After the black lamps were switched off, the formed aerosols were characterized for another 0.5 h to correct the wall loss [29]. More details can be found in Text S2 and Figure S2. In the ambient air matrix experiments, ambient air was introduced into the reactor with a pump, while other initial conditions and reaction precursors were similar to the purified air experiments.

In the ambient air matrix experiments, the experimental results may be affected by other precursors that could form SOA during photooxidation. Therefore, an ambient air matrix blank experiment was conducted. All operating procedures and conditions in the blank experiment (Table 1) were similar to those of the ambient air matrix experiments, except for the absence of  $\alpha$ -pinene. An SOA of  $2.4$   $\mu\text{g m}^{-3}$  in the blank experiment was formed, accounting for less than 1% of SOA formed in the presence of  $\alpha$ -pinene during ambient air matrix experiments. This indicates that the influence of other SOA precursors could be neglected in the ambient air matrix experiments.

## 2.2. Instrumentation

A series of online instruments were used in the experiments to characterize the gas and aerosol phase compounds in the reactor. A Model 49i analyzer (Thermo Scientific, Waltham, MA, USA) was used to measure O<sub>3</sub>. A Model 42i analyzer (Thermo Scientific, Waltham, MA, USA) was used to measure NO<sub>x</sub>. A Model 43i analyzer (Thermo Scientific, Waltham, MA, USA) was used to measure SO<sub>2</sub>. Volatile organic compounds (VOCs) were measured using a proton-transfer-reaction time-of-flight mass spectrometer (PTR-ToF-MS, Fusion PTR-ToF 10k, Ionicon Analytik GmbH, Innsbruck, Austria). The PTR-ToF-MS was calibrated before the experiments and more details about the calibration and data manipulation can be found in Text S3 and Figure S3. Particle number concentrations and size distributions were measured with a scanning mobility particle sizer (SMPS, Model 3080 classifier, Model 3775 CPC; TSI Inc., Shoreview, MN, USA). Mass concentrations and chemical compositions of particles were measured using a high-resolution time-of-flight aerosol mass spectrometer (HR-ToF-MS, Aerodyne Research Inc., Billerica, MA, USA). The HR-ToF-AMS was calibrated using 400 nm monodisperse ammonium nitrate aerosols and more details can be found in Text S4 and Figure S4.

### 3. Results and Discussion

#### 3.1. Evolutions of Gas-Phase Species during Photooxidation

As shown in Figure 1, concentrations of trace gases (NO, NO<sub>2</sub>, O<sub>3</sub>, and SO<sub>2</sub>) and  $\alpha$ -pinene changed in a similar pattern during photooxidation in the purified air and ambient air matrix experiments except for the inconsistent pace. During the initial stage of photooxidation, the  $\alpha$ -pinene concentrations decreased slowly, and declined much faster when the NO concentration neared 0. The O<sub>3</sub> level started to accumulate when the NO concentration decreased to nearly 0, reaching quickly its maximum and then decreasing slowly. Previous studies have demonstrated that SOA could be produced through the reaction of  $\alpha$ -pinene with O<sub>3</sub> [12,30–32]. Therefore, the decreasing rates were determined not only by oxidation of OH radicals, but also more and more by O<sub>3</sub>, which was accumulating during photooxidation.

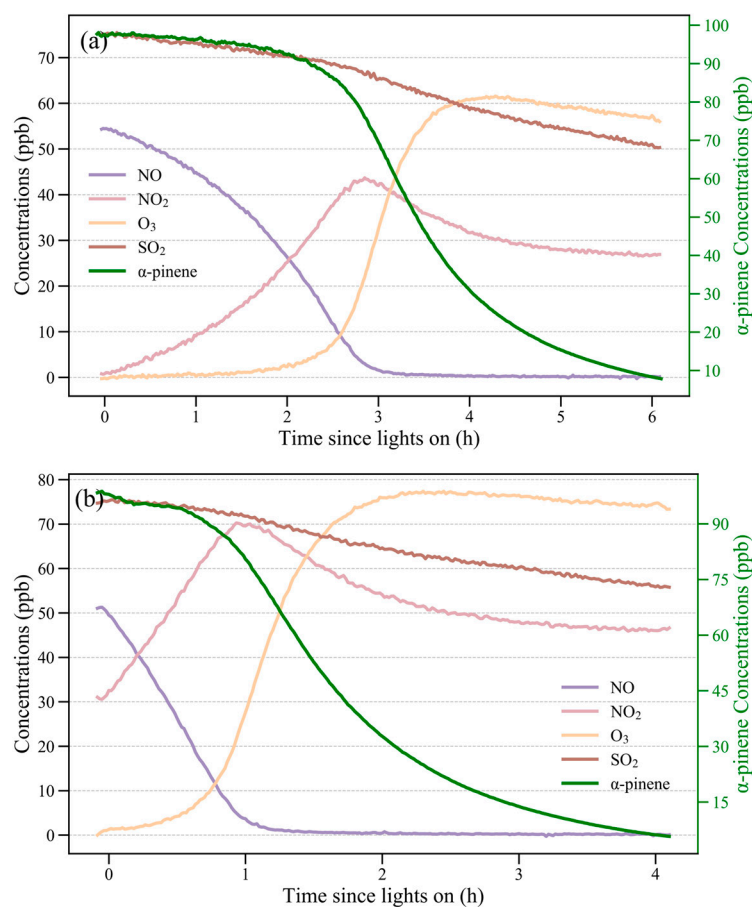


**Figure 1.** Changes in levels of trace gases (NO, NO<sub>2</sub>, SO<sub>2</sub>, and O<sub>3</sub>) during photooxidation: (a) in a purified air and (b) in an ambient air matrix experiment.

Major oxidation products in the gas-phase were measured by PTR-ToF-MS. Table 2 shown their yields expressed as the ratios of their production to consumed  $\alpha$ -pinene. The production of higher molecular weight compounds seemed to be lower in the ambient air matrix experiments, probably due to higher molecular weight compounds being less volatile and more likely to enter the aerosol phase by gas-particle partitioning in ambient air in the presence of initial aerosols. As shown in Figure 2 and according to previous studies, the detected most prominent oxidation products were acetone ( $m/z$  59), acetic acid ( $m/z$  61), and pinonaldehyde ( $m/z$  169) [33–35]. The acetone yields ( $0.49 \pm 0.02$ ) in the ambient air matrix experiments were close to that of  $0.50 \pm 0.04$  in purified air experiments, while the acetic acid yields ( $0.13 \pm 0.05$ ) were higher than that of  $0.09 \pm 0.01$  in the purified air experiments, and yields of pinonaldehyde ( $\sim 0.24$ ) were slightly higher than that of  $\sim 0.20$  in the purified air experiments. Pinonaldehyde could be further oxidized

to form smaller volatile organic compounds such as acetone during the photooxidation of  $\alpha$ -pinene [35,36]. Higher pinonaldehyde yields and lower acetone yields in the ambient air matrix experiments might also indicate that pinonaldehyde is more likely to be oxidized to form low volatility compounds and promote SOA formation in ambient air.

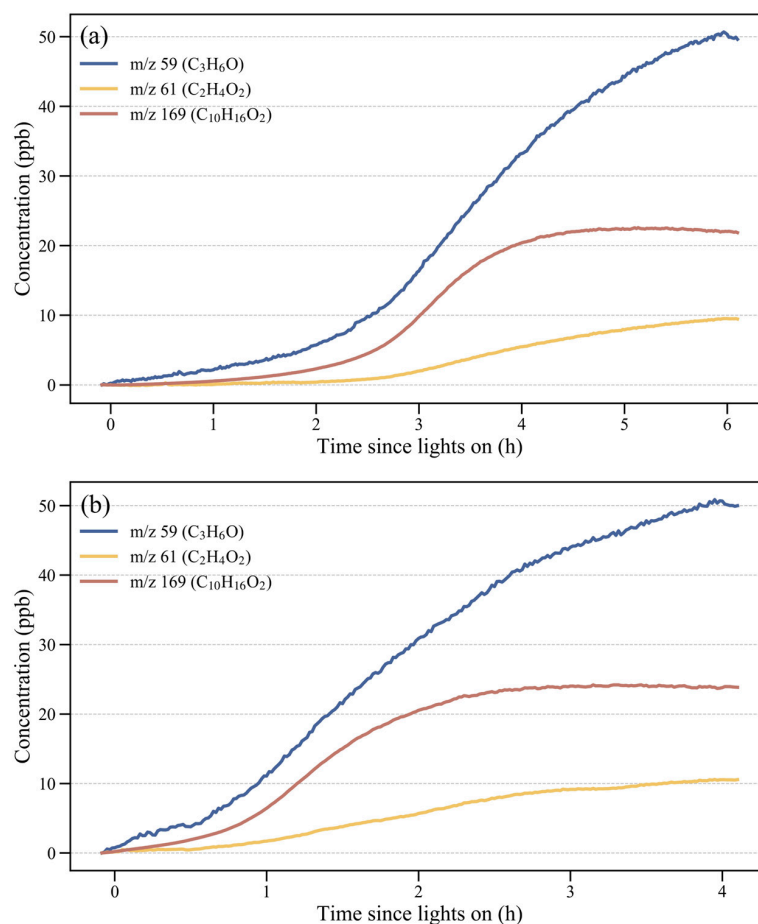


**Figure 2.** Changing concentrations of acetone ( $m/z$  59), acetic acid ( $m/z$  61), and pinonaldehyde ( $m/z$  169) during photooxidation: (a) in a purified air matrix experiment and (b) in an ambient air matrix experiment.

**Table 2.** Yields of gas-phase oxidation products expressed as the ratio ( $\times 10^{-2}$  or %) of their production to the consumed  $\alpha$ -pinene as measured by PTR-ToF-MS. Formulas are inferred from the oxidation pathways of  $\alpha$ -pinene in the MCM mechanism [37].

$m/z$	Formula	Ambient Air	Purified Air
31	CH <sub>2</sub> O	1.0 ± 0.2	0.7 ± 0.1
59	C <sub>3</sub> H <sub>6</sub> O	48.9 ± 1.7	50.4 ± 4.2
61	C <sub>2</sub> H <sub>4</sub> O <sub>2</sub>	13.3 ± 5.1	9.4 ± 1.3
73	C <sub>3</sub> H <sub>4</sub> O <sub>2</sub>	2.1 ± 0.9	1.7 ± 0.9
77	C <sub>2</sub> H <sub>4</sub> O <sub>3</sub>	1.2 ± 0.1	1.3 ± 0.1
87	C <sub>3</sub> H <sub>2</sub> O <sub>3</sub>	3.0 ± 0.7	1.9 ± 0.0
89	C <sub>3</sub> H <sub>4</sub> O <sub>3</sub>	0.6 ± 1.1	0.4 ± 0.4
101	C <sub>4</sub> H <sub>4</sub> O <sub>3</sub>	0.2 ± 0.9	0.4 ± 0.1
103	C <sub>4</sub> H <sub>6</sub> O <sub>3</sub>	0.1 ± 0.0	0.1 ± 0.0
115	C <sub>5</sub> H <sub>6</sub> O <sub>3</sub>	1.5 ± 0.3	1.3 ± 0.2
117	C <sub>5</sub> H <sub>8</sub> O <sub>3</sub> , C <sub>4</sub> H <sub>4</sub> O <sub>4</sub>	0.1 ± 0.5	0.3 ± 0.1
119	C <sub>4</sub> H <sub>6</sub> O <sub>4</sub>	0.1 ± 0.5	0.3 ± 0.0
133	C <sub>5</sub> H <sub>8</sub> O <sub>4</sub> , C <sub>4</sub> H <sub>4</sub> O <sub>5</sub>	0.6 ± 0.1	0.7 ± 0.0
135	C <sub>4</sub> H <sub>6</sub> O <sub>5</sub>	1.3 ± 0.2	1.3 ± 0.2

Table 2. Cont.

<i>m/z</i>	Formula	Ambient Air	Purified Air
143	C <sub>8</sub> H <sub>14</sub> O <sub>2</sub> , C <sub>6</sub> H <sub>6</sub> O <sub>4</sub>	0.3 ± 0.1	0.3 ± 0.0
147	C <sub>6</sub> H <sub>10</sub> O <sub>4</sub> , C <sub>5</sub> H <sub>6</sub> O <sub>5</sub>	0.2 ± 0.0	0.2 ± 0.0
155	C <sub>9</sub> H <sub>14</sub> O <sub>2</sub>	1.6 ± 0.2	1.8 ± 0.2
157	C <sub>7</sub> H <sub>8</sub> O <sub>4</sub> , C <sub>8</sub> H <sub>12</sub> O <sub>3</sub> , C <sub>9</sub> H <sub>16</sub> O <sub>2</sub>	0.6 ± 0.2	0.6 ± 0.0
159	C <sub>7</sub> H <sub>10</sub> O <sub>4</sub> , C <sub>8</sub> H <sub>14</sub> O <sub>3</sub>	0.1 ± 0.0	0.1 ± 0.0
161	C <sub>7</sub> H <sub>12</sub> O <sub>4</sub>	0.04 ± 0.02	0.05 ± 0.04
169	C <sub>10</sub> H <sub>16</sub> O <sub>2</sub>	23.8 ± 2.9	19.8 ± 7.2
171	C <sub>9</sub> H <sub>14</sub> O <sub>3</sub> , C <sub>10</sub> H <sub>18</sub> O <sub>2</sub>	0.6 ± 0.1	0.6 ± 0.1
173	C <sub>9</sub> H <sub>16</sub> O <sub>3</sub>	0.2 ± 0.0	0.1 ± 0.0
175	C <sub>8</sub> H <sub>14</sub> O <sub>4</sub> , C <sub>7</sub> H <sub>10</sub> O <sub>5</sub>	0.03 ± 0.01	0.04 ± 0.00
183	C <sub>10</sub> H <sub>14</sub> O <sub>3</sub>	0.9 ± 0.1	1.1 ± 0.0
185	C <sub>10</sub> H <sub>16</sub> O <sub>3</sub>	0.7 ± 0.1	0.8 ± 0.1
187	C <sub>9</sub> H <sub>14</sub> O <sub>4</sub> , C <sub>10</sub> H <sub>18</sub> O <sub>3</sub>	0.1 ± 0.0	0.1 ± 0.0
189	C <sub>9</sub> H <sub>16</sub> O <sub>4</sub> , C <sub>7</sub> H <sub>8</sub> O <sub>6</sub> , C <sub>8</sub> H <sub>12</sub> O <sub>5</sub>	0.01 ± 0.01	0.01 ± 0.00
201	C <sub>10</sub> H <sub>16</sub> O <sub>4</sub>	0.05 ± 0.01	0.03 ± 0.01

### 3.2. SOA Formation during Photooxidation

In the purified air matrix experiments, new particles formed and the particle number concentrations increased after about 1 h of photooxidation, reaching the maximums after 3 h of photooxidation (Figure 3a). Meanwhile organic aerosol concentrations remained negligible for the first 3 h, increased rapidly thereafter, and then leveled off (Figure 4). The purified air matrix experiments were conducted without seed aerosols and the oxidation products such as pinonaldehyde during photooxidation were hard to nucleate with high volatility [15,38]. Consequently, nucleation did not occur before the oxidation products were further oxidized to form low volatile organic compounds such as dimers [20,25,39,40]. The NO could inhibit the SOA formation in the initial photooxidation stages as the formation of low volatile organic compounds, such as dimers, was inhibited by the reaction of NO with RO<sub>2</sub>, which is not conducive to nucleation and growth [19].

Based on the reaction rate constants of  $\alpha$ -pinene with OH and O<sub>3</sub> ( $k_{OH} = 5.3 \times 10^{-11}$  cm<sup>3</sup> molecule<sup>-1</sup> s<sup>-1</sup>;  $k_{O_3} = 8.9 \times 10^{-17}$  cm<sup>3</sup> molecule<sup>-1</sup> s<sup>-1</sup>) and with measured O<sub>3</sub> concentrations or derived OH concentrations, the percentages of  $\alpha$ -pinene consumed by O<sub>3</sub> or OH radicals could be calculated (Figure 3b). As the NO concentrations neared 0 and O<sub>3</sub> was accumulating, an increasing percentage of  $\alpha$ -pinene was consumed by O<sub>3</sub>. Therefore, the increase in SOA concentrations might be largely due to the production of low volatility and highly oxygenated organic molecules through the reaction between O<sub>3</sub> and  $\alpha$ -pinene [12,32,40,41]. In the ambient air matrix experiments, organic aerosol concentrations started to increase earlier than in the purified air experiments. As shown in Table 1, aerosols were initially present before the  $\alpha$ -pinene photooxidation. As a result, the initial growth in aerosol concentration was observed in the ambient air matrix experiments (Figure 4), possibly due to the condensation of low volatile organic compounds on the aerosols [20]. More importantly, the earlier climb of organic aerosols might be related to the earlier climb of O<sub>3</sub> in the ambient air matrix experiments due to the considerable initial levels of NO<sub>2</sub>.

Changing concentrations of particulate-phase organic aerosols (Org), sulfate (SO<sub>4</sub><sup>2-</sup>), nitrate (NO<sub>3</sub><sup>-</sup>), ammonium (NH<sub>4</sub><sup>+</sup>), and chloride (Chl) could be measured online with the HR-ToF-AMS (Figure 4). Chl accounted for 0.2 ± 0.1% of the aerosol mass in the experiments and thus was negligible in the experiments. As shown in Figure 4, the aerosol components evolved in a similar pattern and shared similar proportions in the purified air and ambient air matrix experiments except that the aerosols formed at a slower pace in the purified air matrix experiments. Org was the most abundant component, accounting for 80.1 ± 1.5% (purified air) and 81.7 ± 3.7% (ambient air) of aerosol mass, followed by sulfate (14.1 ± 1.2% in purified air and 13.1 ± 3.1% in ambient air).

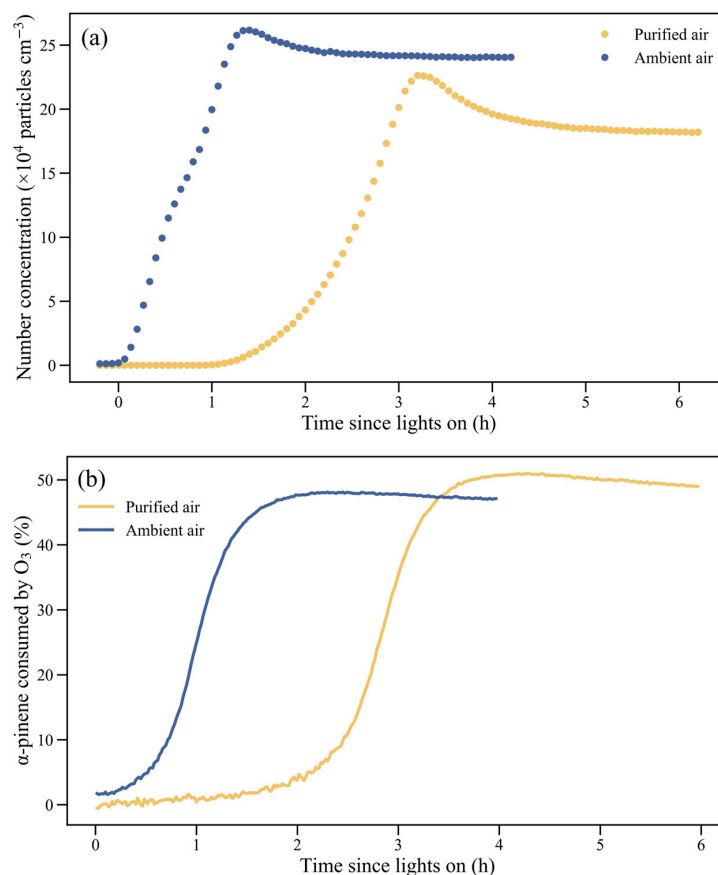


**Figure 3.** Variation of (a) aerosol number concentration and (b) percentage of  $\alpha$ -pinene consumed by  $\text{O}_3$  during photooxidation in a purified air and an ambient air matrix experiment.

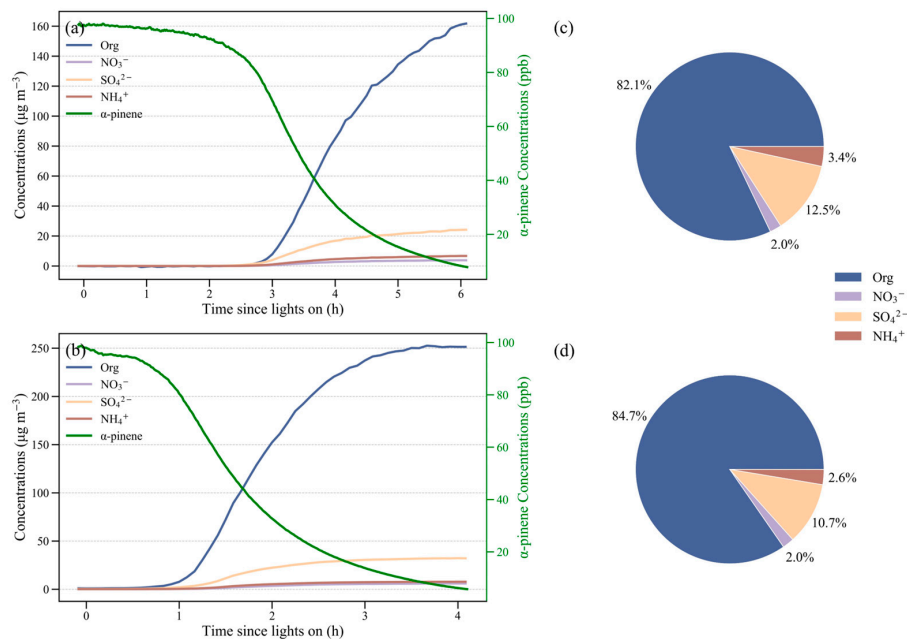


**Figure 4.** Concentration changes of  $\alpha$ -pinene and aerosol components (Org,  $\text{NO}_3^-$ ,  $\text{SO}_4^{2-}$ , and  $\text{NH}_4^+$ ) in (a) a purified air and (b) an ambient air matrix experiment, and the percentage of aerosol components (c) in the purified air and (d) ambient air matrix experiments.

A comparison of SOA yields in this study with those previously reported is presented in Table 3. The average yield of SOA for  $\alpha$ -pinene was  $32.4 \pm 0.4\%$  in our purified air

matrix experiments and  $42.7 \pm 5.3\%$  in our ambient air matrix experiments. The average yield of  $\alpha$ -pinene SOA in our purified air matrix experiments was higher than that in the presence of NO<sub>x</sub> in the previous chamber studies, and closer to those in the absence of NO<sub>x</sub> [24,42–44]. While NO could promote the formation of highly volatile organic compounds by changing the reaction pathway of RO<sub>2</sub> and inhibiting the formation of new particles and SOA [19,20,43], SO<sub>2</sub> could promote the conversion of gas-phase organic compounds entering to the aerosol phase, increasing the SOA yield [20]. As shown in Figure 5, the SOA yield in the ambient air matrix experiments was about 32% higher than that in the purified air. The average growth rate of SOA ( $132.1 \pm 15.7 \mu\text{g m}^{-3} \text{h}^{-1}$ ) in the ambient air matrix experiments was higher than that of  $92.4 \pm 14.5 \mu\text{g m}^{-3} \text{h}^{-1}$  in purified air. The surface area concentration of SOA at the end of the  $\alpha$ -pinene photooxidation stage was  $5924 \pm 475 \mu\text{m}^2 \text{cm}^{-3}$  in the ambient air, higher than  $3831 \pm 536 \mu\text{m}^2 \text{cm}^{-3}$  in the purified air matrix experiments. In the ambient air matrix experiments, higher SOA yields from the  $\alpha$ -pinene photooxidation were associated with higher surface area concentrations of initial seed aerosols (Table 1). Since seed aerosols during the  $\alpha$ -pinene photooxidation could provide a condensation surface and promote the condensation of the low volatile organic compounds to enter the aerosol phase [43,45,46], the growth of Org was earlier in the ambient air matrix experiments, and the average growth rate of SOA and the SOA yield were also higher than those in the purified air matrix experiments. Apart from the role of seed aerosols in the ambient air, the reaction between  $\alpha$ -pinene and O<sub>3</sub>, as well as aerosol acidity, might be factors that led to the differences.

**Table 3.** SOA yields for  $\alpha$ -pinene photooxidation from this study in comparison to those previously reported in the literature.

T (°C)	RH (%)	Oxidant	Seed	[NO] <sub>0</sub> (ppb)	[ $\alpha$ -Pinene] <sub>0</sub> (ppb)	SOA Yield (%)	Reference
25.4 ± 0.3	46.4 ± 2.8	H <sub>2</sub> O <sub>2</sub> + NO <sub>x</sub>	– <sup>b</sup>	53.7 ± 1.1	110.9 ± 12.2	32.4 ± 0.4	This study
25.2 ± 0.5	47.0 ± 6.9	H <sub>2</sub> O <sub>2</sub> + NO <sub>x</sub>	ambient air	51.9 ± 1.9	100.6 ± 1.8	42.7 ± 5.3	
25	<5	H <sub>2</sub> O <sub>2</sub>	–	–	1028.6	21.8	
25	<5	H <sub>2</sub> O <sub>2</sub> + NO <sub>x</sub>	–	1064	1126.4	9.2	[44]
24–26	64–67	H <sub>2</sub> O <sub>2</sub>	AS <sup>a</sup>	<0.3	17.4–19.6	28.6–36.3	[43]
23–26	47–61	H <sub>2</sub> O <sub>2</sub> + NO <sub>x</sub>	AS	66–72	13.6–17.6	4.2–7.6	
20–23	<10	H <sub>2</sub> O <sub>2</sub>	none, AS	–	45.0–48.5	26.7–28.9	[24]
20–23	<10	HONO	none, AS	–	45.5–52.4	7.7–17.6	
20	5.3–6.2	H <sub>2</sub> O <sub>2</sub>	AS	0–1	13.8–47.5	37.9–45.8	[42]
20	6.4	H <sub>2</sub> O <sub>2</sub> + NO <sub>x</sub>	AS	198	13.1	21.2	

<sup>a</sup> AS is ammonium sulfate. <sup>b</sup> – indicates that it was not added in the experiments.

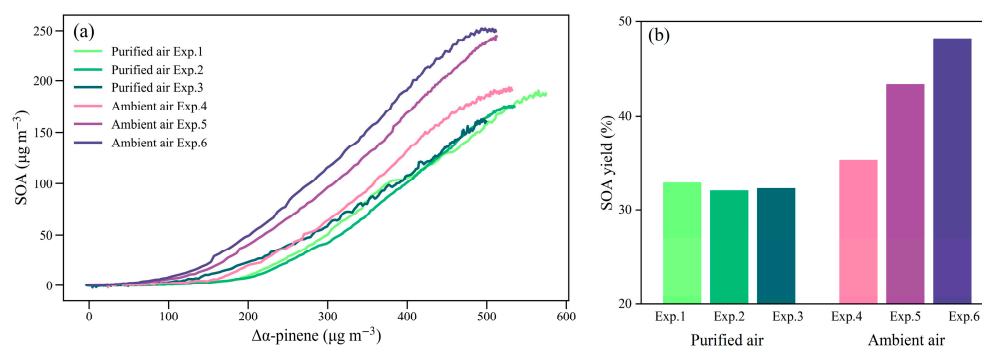


**Figure 5.** Changing concentrations of SOA from  $\alpha$ -pinene photooxidation (a) and SOA yield (b) in the purified air and ambient air matrix experiments.

Previous studies have suggested that the formation of SOA from  $\alpha$ -pinene photooxidation could be affected by SO<sub>2</sub> through acid-catalyzed reactions [20,47]. The carbonyl compounds produced during  $\alpha$ -pinene photooxidation, such as pinonaldehyde, could form

low volatile organic compounds through heterogeneous reactions on the acidic aerosol surface and thus promote SOA formation [31,43,48,49]. In this study, the in-situ acidity ( $H^+$  concentration) of aerosols was calculated by the ISORROPIA-II model [50]. The forward mode and metastable state were applied, in which the total concentrations of  $NO_3^-$  and  $NH_4^+$  in the gas and aerosol phases,  $SO_4^{2-}$  concentration in the aerosol phase, temperature, and RH were used as the input parameters (Table S1). As shown in Figure 6, the in-situ acidity at the end of the  $\alpha$ -pinene photooxidation was  $2.13 \pm 0.41 \text{ nmol m}^{-3}$  in the purified air matrix experiments. In the ambient air matrix experiments, the in-situ acidity of the aerosol was initially  $0.32 \pm 0.09 \text{ nmol m}^{-3}$  and reached  $12.44 \pm 2.07 \text{ nmol m}^{-3}$  at the end of photooxidation. The in-situ acidity at the end of photooxidation in the ambient air matrix experiments was nearly six times higher than that in the purified air matrix experiments. The  $\alpha$ -pinene SOA yield was correlated almost linearly with aerosol acidity in the photooxidation reaction with  $NO_x$  [43]. The higher SOA yield in the ambient air matrix experiments might be largely due to the higher in-situ acidity. The liquid water content of the aerosols was also calculated by the ISORROPIA-II model and is shown in Table S1. The aerosol water content was  $30.2 \pm 6.9 \text{ } \mu\text{g m}^{-3}$  in the purified air and  $26.8 \pm 15.1 \text{ } \mu\text{g m}^{-3}$  in the ambient air matrix experiments. The aerosol water contents were quite similar in the ambient air and purified air matrix experiments, indicating that the aerosol water content might not be the limiting factor to SOA formation in this study.

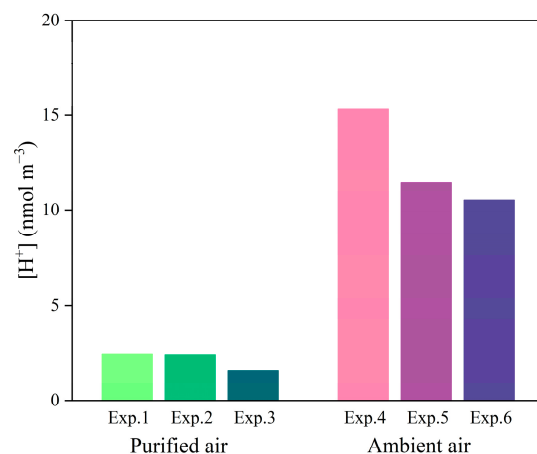


**Figure 6.** In-situ acidity during  $\alpha$ -pinene photooxidation in the purified air and ambient air matrix experiments.

### 3.3. SOA Compositions Measured by HR-ToF-AMS

The SOA mass spectra obtained from HR-ToF-AMS are presented in Figure 7. The ions were classified into  $C_xH_y$ ,  $C_xH_yO$ ,  $C_xH_yO_{>1}$ , and  $C_xH_yO_zN$  families ( $x, y, z \geq 1$ ) according to their elemental contents. In the purified air matrix experiments,  $C_xH_y$  constituted  $48.1 \pm 0.3\%$  of the total signal, followed by  $C_xH_yO$  ( $38.3 \pm 0.6\%$ ),  $C_xH_yO_{>1}$  ( $11.8 \pm 0.4\%$ ), and  $C_xH_yO_zN$  ( $1.8 \pm 0.9\%$ ). The oxygen fragments  $C_xH_yO$  and  $C_xH_yO_{>1}$  together constituted  $50.1 \pm 1.0\%$  of the total signal. Compared to the purified air matrix experiments, the  $C_xH_y$  signal in the ambient air matrix experiments was higher ( $53.7 \pm 1.1\%$ ) and the total  $C_xH_yO$  and  $C_xH_yO_{>1}$  ( $45.0 \pm 0.9\%$ ) was lower, indicating that the SOA formed in the ambient air was less oxidized than in the purified air. The average OH concentration in the ambient air matrix experiments was higher than that in the purified air (Table 1), but the oxidation stage of SOA did not increase with the increase in the average OH concentration. This further indicated that the initial seed aerosols could promote the formation of SOA through facilitating the gas-particle partitioning of low volatile organic compounds, and in the purified air matrix experiments more oxidized and lower volatile organic compounds are needed for nucleation and SOA formation [20,25,39,40]. As shown in Figure 8, the ratio of O:C in the ambient air matrix experiments was  $0.41 \pm 0.01$  on average, lower than  $0.46 \pm 0.01$  in the purified air, further implying that the oxidation stage of the formed

SOA in the ambient air was lower than that in the purified air. As shown in Figure 7, the most distinctive ion was  $C_2H_3O^+$ , followed by  $CO_2^+$  in the purified air and ambient air matrix experiments.  $C_2H_3O^+$  consisted of fragments of non-acidic compounds such as alcohols, aldehydes, and ketones formed through the reaction of  $RO_2$  and  $NO$  [15,41].  $CO_2^+$  consisted of fragments of acidic oxygenated compounds such as acids and esters [51]. Therefore, the similar fragment ion distribution with distinctive ions of  $C_2H_3O^+$  and  $CO_2^+$  indicated that the SOA formed in the photochemical reaction of  $\alpha$ -pinene +  $NO$  +  $SO_2$  might be mainly alcohols, aldehydes, and ketones.

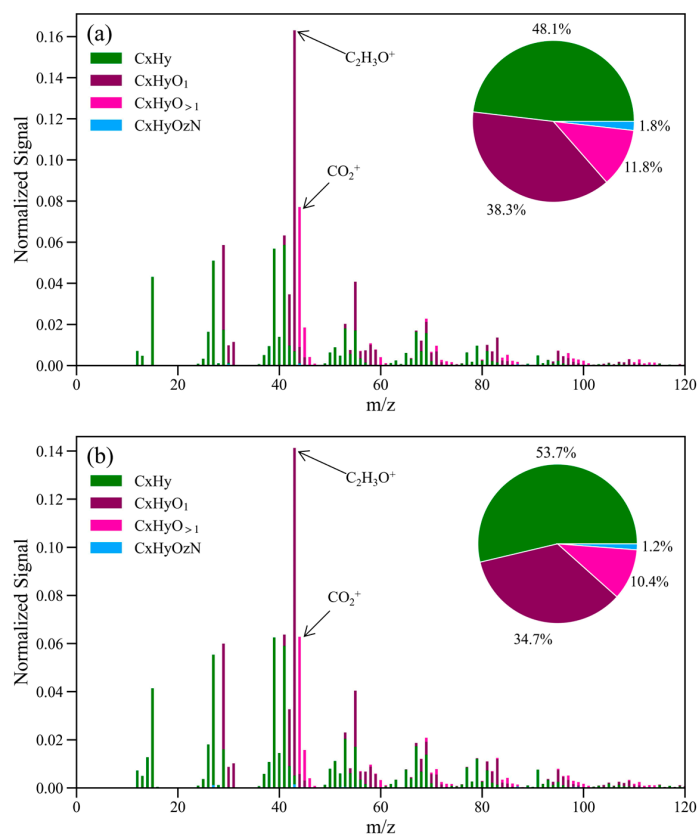


**Figure 7.** The SOA mass spectra obtained from HR-ToF-AMS during  $\alpha$ -pinene photooxidation: (a) in a purified air and (b) an ambient air matrix experiment, with the total signal normalized to 1.0. The insets in (a,b) represent the percentage of  $C_xH_y$ ,  $C_xH_yO$ ,  $C_xH_yO_{>1}$ , and  $C_xH_yO_zN$  ( $x, y, z \geq 1$ ) in a purified air and an ambient air matrix experiment.

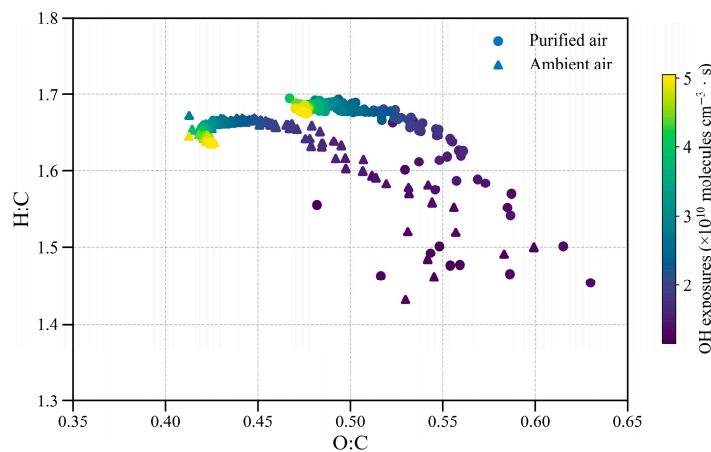


**Figure 8.** Van Krevelen diagram of SOA formed during  $\alpha$ -pinene photooxidation in a purified air and an ambient air matrix experiment.

#### 4. Conclusions

In this study, chamber experiments of  $\alpha$ -pinene photooxidation in the presence of NO and SO<sub>2</sub> were conducted under purified air and ambient air conditions. SOA formation occurred earlier in the ambient air matrix experiments than in the purified air. This might be due to the fact that the low volatile organic compounds formed by  $\alpha$ -pinene oxidation could condense on the initial aerosols. The  $\alpha$ -pinene SOA yield in the ambient air matrix experiments was  $42.7 \pm 5.3\%$ , higher than  $32.4 \pm 0.4\%$  in the purified air. The SOA showed a higher percentage of C<sub>x</sub>H<sub>y</sub> and less C<sub>x</sub>H<sub>y</sub>O and C<sub>x</sub>H<sub>y</sub>O<sub>>1</sub> in the ambient air matrix experiments than in the purified air matrix experiments, and the O:C ratio in the ambient air matrix experiments was  $0.41 \pm 0.01$ , lower than  $0.46 \pm 0.01$  in the purified air. The higher SOA yield in the ambient air could be attributed to the initial aerosol, which facilitates low volatile organic compounds to enter the aerosol phase through gas-particle partitioning, and to higher aerosol acidity. The in-situ aerosol acidity calculated by the ISORROPIA-II model in the ambient air matrix experiments was  $12.44 \pm 2.07 \text{ nmol m}^{-3}$ , higher than that of  $2.13 \pm 0.41 \text{ nmol m}^{-3}$  in the purified air. The most distinctive ion of SOA was C<sub>2</sub>H<sub>3</sub>O<sup>+</sup> in the purified air and ambient air matrix experiments, indicating that the SOA were compounds with carbonyl and hydroxyl functional groups.

In this study, we have only reported preliminary results from our chamber simulations. More in-depth investigations are needed, such as challenging the box model results with the measured changes in gas- and particle-phase compositions, and characterizing and differentiating the SOA formed in purified air and ambient air with more advanced techniques like Fourier transform ion cyclotron resonance mass spectrometry (FT-ICR-MS) [52,53]. In this study, the ambient air we introduced was relatively clean with an organic aerosol mass less than  $1.5 \mu\text{g m}^{-3}$ , and the SO<sub>2</sub> levels were much higher than the levels commonly detected in the ambient air. Thus, in the future, more practical ambient air matrices and pollutant combinations should be considered.

**Supplementary Materials:** The following supporting information can be downloaded at: <https://www.mdpi.com/article/10.3390/atmos15020204/s1>, Text S1: Determination of OH concentration; Text S2: Wall loss correction; Text S3: Calibration of PTR-ToF-MS; Text S4: Calibration of HR-ToF-AMS; Table S1: Input data of ISORROPIA-II model and liquid water content (LWC) calculated by the model; Figure S1: Average OH concentration in the experiment; Figure S2: Trends in organic aerosol (OA) mass concentration before and after wall loss correction in a purified air (a) and an ambient air matrix experiment (b); Figure S3: The calibration curve of  $\alpha$ -pinene measured by PTR-ToF-MS; Figure S4: The IE calibration fitting curve for HR-ToF-AMS. Refs. [28,29] are cited in the Supplementary materials.

**Author Contributions:** Methodology, X.L. and X.W.; validation, X.L.; formal analysis, X.L.; investigation, X.L., Z.R., X.Z. and X.P.; data curation, X.L., W.S. and Y.Z.; writing—original draft preparation, X.L.; writing—review and editing, X.W.; visualization, X.L.; supervision, X.W. All authors have read and agreed to the published version of the manuscript.

**Funding:** This study was funded by the Guangdong Foundation for the Program of Science and Technology Research (Grant No. 2023B1212060049) and the Guangzhou Municipal Science and Technology Bureau (Grant No. 202206010057).

**Institutional Review Board Statement:** Not applicable.

**Informed Consent Statement:** Not applicable.

**Data Availability Statement:** The data presented in this study are available on request from the corresponding author. The data are not publicly available due to internal policy of the university.

**Conflicts of Interest:** The authors declare no conflicts of interest. The funders had no role in the design of the study; in the collection, analyses, or interpretation of data; in the writing of the manuscript; or in the decision to publish the results.

## References

1. Hallquist, M.; Wenger, J.C.; Baltensperger, U.; Rudich, Y.; Simpson, D.; Claeys, M.; Dommen, J.; Donahue, N.M.; George, C.; Goldstein, A.H.; et al. The formation, properties and impact of secondary organic aerosol: Current and emerging issues. *Atmos. Chem. Phys.* **2009**, *9*, 5155–5236. [[CrossRef](#)]
2. Cohen, A.J.; Brauer, M.; Burnett, R.; Anderson, H.R.; Frostad, J.; Estep, K.; Balakrishnan, K.; Brunekreef, B.; Dandona, L.; Dandona, R.; et al. Estimates and 25-year trends of the global burden of disease attributable to ambient air pollution: An analysis of data from the global burden of diseases study 2015. *Lancet* **2017**, *389*, 1907–1918. [[CrossRef](#)] [[PubMed](#)]
3. Kelly, J.M.; Doherty, R.M.; O'Connor, F.M.; Mann, G.W. The impact of biogenic, anthropogenic, and biomass burning volatile organic compound emissions on regional and seasonal variations in secondary organic aerosol. *Atmos. Chem. Phys.* **2018**, *18*, 7393–7422. [[CrossRef](#)]
4. Cao, J.; Situ, S.; Hao, Y.; Xie, S.; Li, L. Enhanced summertime ozone and SOA from biogenic volatile organic compound (BVOC) emissions due to vegetation biomass variability during 1981–2018 in China. *Atmos. Chem. Phys.* **2022**, *22*, 2351–2364. [[CrossRef](#)]
5. Guenther, A.B.; Jiang, X.; Heald, C.L.; Sakulyanontvittaya, T.; Duhl, T.; Emmons, L.K.; Wang, X. The model of emissions of gases and aerosols from nature version 2.1 (MEGAN2.1): An extended and updated framework for modeling biogenic emissions. *Geosci. Model Dev.* **2012**, *5*, 1471–1492. [[CrossRef](#)]
6. Ding, X.; Zhang, Y.Q.; He, Q.F.; Yu, Q.Q.; Shen, R.Q.; Zhang, Y.; Zhang, Z.; Lyu, S.J.; Hu, Q.H.; Wang, Y.S.; et al. Spatial and seasonal variations of secondary organic aerosol from terpenoids over China. *J. Geophys. Res. Atmos.* **2016**, *121*, 14–661–14–678. [[CrossRef](#)]
7. Zhang, H.; Yee, L.D.; Lee, B.H.; Curtis, M.P.; Worton, D.R.; Isaacman-VanWertz, G.; Offenberg, J.H.; Lewandowski, M.; Kleindienst, T.E.; Beaver, M.R.; et al. Monoterpenes are the largest source of summertime organic aerosol in the southeastern United States. *Proc. Natl. Acad. Sci. USA* **2018**, *115*, 2038–2043. [[CrossRef](#)]
8. Pai, S.J.; Heald, C.L.; Pierce, J.R.; Farina, S.C.; Marais, E.A.; Jimenez, J.L.; Campuzano-Jost, P.; Nault, B.A.; Middlebrook, A.M.; Coe, H.; et al. An evaluation of global organic aerosol schemes using airborne observations. *Atmos. Chem. Phys.* **2020**, *20*, 2637–2665. [[CrossRef](#)]
9. Zheng, Y.; Horowitz, L.W.; Menzel, R.; Paynter, D.J.; Naik, V.; Li, J.; Mao, J. Anthropogenic amplification of biogenic secondary organic aerosol production. *Atmos. Chem. Phys.* **2023**, *23*, 8993–9007. [[CrossRef](#)]
10. Sindelarova, K.; Markova, J.; Simpson, D.; Huszar, P.; Karlicky, J.; Darras, S.; Granier, C. High-resolution biogenic global emission inventory for the time period 2000–2019 for air quality modelling. *Earth Syst. Sci. Data* **2022**, *14*, 251–270. [[CrossRef](#)]
11. Saha, P.K.; Grieshop, A.P. Exploring divergent volatility properties from yield and thermodenuder measurements of secondary organic aerosol from  $\alpha$ -pinene ozonolysis. *Environ. Sci. Technol.* **2016**, *50*, 5740–5749. [[CrossRef](#)] [[PubMed](#)]
12. Kristensen, K.; Jensen, L.N.; Quéléver, L.L.J.; Christiansen, S.; Rosati, B.; Elm, J.; Teiwes, R.; Pedersen, H.B.; Glasius, M.; Ehn, M.; et al. The Aarhus chamber campaign on highly oxygenated organic molecules and aerosols (ACCHA): Particle formation, organic acids, and dimer esters from  $\alpha$ -pinene ozonolysis at different temperatures. *Atmos. Chem. Phys.* **2020**, *20*, 12549–12567. [[CrossRef](#)]
13. Chu, C.-W.; Zhai, J.; Han, Y.; Ye, J.; Zaveri, R.A.; Martin, S.T.; Hung, H.-M. New particle formation and growth dynamics for  $\alpha$ -pinene ozonolysis in a smog chamber and Implications for ambient environments. *ACS Earth Space Chem.* **2022**, *6*, 2826–2835. [[CrossRef](#)]
14. Day, D.A.; Fry, J.L.; Kang, H.G.; Krechmer, J.E.; Ayres, B.R.; Keehan, N.I.; Thompson, S.L.; Hu, W.; Campuzano-Jost, P.; Schroder, J.C.; et al. Secondary organic aerosol mass yields from  $\text{NO}_3$  oxidation of  $\alpha$ -pinene and  $\Delta$ -carene: Effect of  $\text{RO}_2$  radical fate. *J. Phys. Chem. A* **2022**, *126*, 7309–7330. [[CrossRef](#)]
15. DeVault, M.P.; Ziola, A.C.; Ziemann, P.J. Chemistry of secondary organic aerosol formation from reactions of monoterpenes with OH radicals in the presence of  $\text{NO}_x$ . *J. Phys. Chem. A* **2022**, *126*, 7719–7736. [[CrossRef](#)]
16. Chu, B.; Liu, T.; Zhang, X.; Liu, Y.; Ma, Q.; Ma, J.; He, H.; Wang, X.; Li, J.; Hao, J. Secondary aerosol formation and oxidation capacity in photooxidation in the presence of  $\text{Al}_2\text{O}_3$  seed particles and  $\text{SO}_2$ . *Sci. China Chem.* **2015**, *58*, 1426–1434. [[CrossRef](#)]
17. Simon, M.; Dada, L.; Heinritzi, M.; Scholz, W.; Stolzenburg, D.; Fischer, L.; Wagner, A.C.; Kürten, A.; Rörup, B.; He, X.-C.; et al. Molecular understanding of new-particle formation from  $\alpha$ -pinene between  $-50$  and  $+25$  °C. *Atmos. Chem. Phys.* **2020**, *20*, 9183–9207. [[CrossRef](#)]
18. Bryant, D.J.; Dixon, W.J.; Hopkins, J.R.; Dunmore, R.E.; Pereira, K.L.; Shaw, M.; Squires, F.A.; Bannan, T.J.; Mehra, A.; Worrall, S.D.; et al. Strong anthropogenic control of secondary organic aerosol formation from isoprene in Beijing. *Atmos. Chem. Phys.* **2020**, *20*, 7531–7552. [[CrossRef](#)]
19. Wildt, J.; Mentel, T.F.; Kiendler-Scharr, A.; Hoffmann, T.; Andres, S.; Ehn, M.; Kleist, E.; Müsgen, P.; Rohrer, F.; Rudich, Y.; et al. Suppression of new particle formation from monoterpene oxidation by  $\text{NO}_x$ . *Atmos. Chem. Phys.* **2014**, *14*, 2789–2804. [[CrossRef](#)]
20. Zhao, D.; Schmitt, S.H.; Wang, M.; Acir, I.-H.; Tillmann, R.; Tan, Z.; Novelli, A.; Fuchs, H.; Pullinen, I.; Wegener, R.; et al. Effects of  $\text{NO}_x$  and  $\text{SO}_2$  on the secondary organic aerosol formation from photooxidation of  $\alpha$ -pinene and limonene. *Atmos. Chem. Phys.* **2018**, *18*, 1611–1628. [[CrossRef](#)]
21. Kleindienst, T.E.; Edney, E.O.; Lewandowski, M.; Offenberg, J.H.; Jaoui, M. Secondary organic carbon and aerosol yields from the irradiations of isoprene and  $\alpha$ -pinene in the presence of  $\text{NO}_x$  and  $\text{SO}_2$ . *Environ. Sci. Technol.* **2006**, *40*, 3807–3812. [[CrossRef](#)] [[PubMed](#)]

22. Friedman, B.; Brophy, P.; Brune, W.H.; Farmer, D.K. Anthropogenic sulfur perturbations on biogenic oxidation: SO<sub>2</sub> additions impact gas-phase OH oxidation products of alpha- and beta-pinene. *Environ. Sci. Technol.* **2016**, *50*, 1269–1279. [[CrossRef](#)] [[PubMed](#)]
23. Ng, N.L.; Kroll, J.H.; Keywood, M.D.; Bahreini, R.; Varutbangkul, V.; Flagan, R.C.; Seinfeld, J.H.; Lee, A.; Goldstein, A.H. Contribution of first-versus second-generation products to secondary organic aerosols formed in the oxidation of biogenic hydrocarbons. *Environ. Sci. Technol.* **2006**, *40*, 2283–2297. [[CrossRef](#)]
24. Eddingsaas, N.C.; Loza, C.L.; Yee, L.D.; Chan, M.; Schilling, K.A.; Chhabra, P.S.; Seinfeld, J.H.; Wennberg, P.O.  $\alpha$ -pinene photooxidation under controlled chemical conditions—Part 2: SOA yield and composition in low- and high-NO<sub>x</sub> environments. *Atmos. Chem. Phys.* **2012**, *12*, 7413–7427. [[CrossRef](#)]
25. Kirkby, J.; Duplissy, J.; Sengupta, K.; Frege, C.; Gordon, H.; Williamson, C.; Heinritzi, M.; Simon, M.; Yan, C.; Almeida, J.; et al. Ion-induced nucleation of pure biogenic particles. *Nature* **2016**, *533*, 521–526. [[CrossRef](#)]
26. Deng, W.; Liu, T.; Zhang, Y.; Situ, S.; Hu, Q.; He, Q.; Zhang, Z.; Lü, S.; Bi, X.; Wang, X.; et al. Secondary organic aerosol formation from photo-oxidation of toluene with NO<sub>x</sub> and SO<sub>2</sub>: Chamber simulation with purified air versus urban ambient air as matrix. *Atmos. Environ.* **2017**, *150*, 67–76. [[CrossRef](#)]
27. Wang, X.; Liu, T.; Bernard, F.; Ding, X.; Wen, S.; Zhang, Y.; Zhang, Z.; He, Q.; Lü, S.; Chen, J.; et al. Design and characterization of a smog chamber for studying gas-phase chemical mechanisms and aerosol formation. *Atmos. Meas. Tech.* **2014**, *7*, 301–313. [[CrossRef](#)]
28. Barmet, P.; Dommen, J.; DeCarlo, P.F.; Tritscher, T.; Praplan, A.P.; Platt, S.M.; Prévôt, A.S.H.; Donahue, N.M.; Baltensperger, U. OH clock determination by proton transfer reaction mass spectrometry at an environmental chamber. *Atmos. Meas. Tech.* **2012**, *5*, 647–656. [[CrossRef](#)]
29. Weitkamp, E.A.; Sage, A.M.; Pierce, J.R.; Donahue, N.M.; Robinson, A.L. Organic aerosol formation from photochemical oxidation of diesel exhaust in a smog chamber. *Environ. Sci. Technol.* **2007**, *41*, 6969–6975. [[CrossRef](#)]
30. Xavier, C.; Rusanen, A.; Zhou, P.; Dean, C.; Pichelstorfer, L.; Roldin, P.; Boy, M. Aerosol mass yields of selected biogenic volatile organic compounds—A theoretical study with nearly explicit gas-phase chemistry. *Atmos. Chem. Phys.* **2019**, *19*, 13741–13758. [[CrossRef](#)]
31. Deng, Y.; Inomata, S.; Sato, K.; Ramasamy, S.; Morino, Y.; Enami, S.; Tanimoto, H. Temperature and acidity dependence of secondary organic aerosol formation from  $\alpha$ -pinene ozonolysis with a compact chamber system. *Atmos. Chem. Phys.* **2021**, *21*, 5983–6003. [[CrossRef](#)]
32. Zhao, J.; Häkkinen, E.; Graeffe, F.; Krechmer, J.E.; Canagaratna, M.R.; Worsnop, D.R.; Kangasluoma, J.; Ehn, M. A combined gas- and particle-phase analysis of highly oxygenated organic molecules (HOMs) from  $\alpha$ -pinene ozonolysis. *Atmos. Chem. Phys.* **2023**, *23*, 3707–3730. [[CrossRef](#)]
33. Hellén, H.; Dommen, J.; Metzger, A.; Gascho, A.; Duplissy, J.; Tritscher, T.; Prevot, A.S.H.; Baltensperger, U. Using proton transfer reaction mass spectrometry for online analysis of secondary organic aerosols. *Environ. Sci. Technol.* **2008**, *42*, 7347–7353. [[CrossRef](#)]
34. Rosati, B.; Teiwes, R.; Kristensen, K.; Bossi, R.; Skov, H.; Glasius, M.; Pedersen, H.B.; Bilde, M. Factor analysis of chemical ionization experiments: Numerical simulations and an experimental case study of the ozonolysis of  $\alpha$ -pinene using a PTR-ToF-MS. *Atmos. Environ.* **2019**, *199*, 15–31. [[CrossRef](#)]
35. Zhang, P.; Ma, P.; Shu, J.; Huang, J.; Yang, B.; Zhang, H. Characterization of crucial fragments during the nucleation and growth of secondary organic aerosol from the high-NO photo-oxidation of  $\alpha$ -pinene. *Atmos. Environ.* **2019**, *213*, 47–54. [[CrossRef](#)]
36. Geddes, S.; Nichols, B.; Todd, K.; Zahardis, J.; Petrucci, G.A. Near-infrared laser desorption/ionization aerosol mass spectrometry for measuring organic aerosol at atmospherically relevant aerosol mass loadings. *Atmos. Meas. Tech.* **2010**, *3*, 1175–1183. [[CrossRef](#)]
37. Jenkin, M.E.; Young, J.C.; Rickard, A.R. The MCM v3.3.1 degradation scheme for isoprene. *Atmos. Chem. Phys.* **2015**, *15*, 11433–11459. [[CrossRef](#)]
38. Lee, A.; Goldstein, A.H.; Kroll, J.H.; Ng, N.L.; Varutbangkul, V.; Flagan, R.C.; Seinfeld, J.H. Gas-phase products and secondary aerosol yields from the photooxidation of 16 different terpenes. *J. Geophys. Res. Atmos.* **2006**, *111*, D17. [[CrossRef](#)]
39. Ehn, M.; Thornton, J.A.; Kleist, E.; Sipila, M.; Junninen, H.; Pullinen, I.; Springer, M.; Rubach, F.; Tillmann, R.; Lee, B.; et al. A large source of low-volatility secondary organic aerosol. *Nature* **2014**, *506*, 476–479. [[CrossRef](#)]
40. Kristensen, K.; Cui, T.; Zhang, H.; Gold, A.; Glasius, M.; Surratt, J.D. Dimers in  $\alpha$ -pinene secondary organic aerosol: Effect of hydroxyl radical, ozone, relative humidity and aerosol acidity. *Atmos. Chem. Phys.* **2014**, *14*, 4201–4218. [[CrossRef](#)]
41. Jia, L.; Xu, Y. The role of functional groups in the understanding of secondary organic aerosol formation mechanism from alpha-pinene. *Sci. Total Environ.* **2020**, *738*, 139831. [[CrossRef](#)]
42. Ng, N.L.; Chhabra, P.S.; Chan, A.W.H.; Surratt, J.D.; Kroll, J.H.; Kwan, A.J.; McCabe, D.C.; Wennberg, P.O.; Sorooshian, A.; Murphy, S.M.; et al. Effect of NO<sub>x</sub> level on secondary organic aerosol (SOA) formation from the photooxidation of terpenes. *Atmos. Chem. Phys.* **2007**, *7*, 5159–5174. [[CrossRef](#)]
43. Han, Y.; Stroud, C.A.; Liggio, J.; Li, S.-M. The effect of particle acidity on secondary organic aerosol formation from  $\alpha$ -pinene photooxidation under atmospherically relevant conditions. *Atmos. Chem. Phys.* **2016**, *16*, 13929–13944. [[CrossRef](#)]
44. Park, J.-H.; Babar, Z.B.; Baek, S.J.; Kim, H.S.; Lim, H.-J. Effects of NO<sub>x</sub> on the molecular composition of secondary organic aerosol formed by the ozonolysis and photooxidation of  $\alpha$ -pinene. *Atmos. Environ.* **2017**, *166*, 263–275. [[CrossRef](#)]
45. Kulmala, M.; Kontkanen, J.; Junninen, H.; Lehtipalo, K.; Manninen, H.E.; Nieminen, T.; Petaja, T.; Sipila, M.; Schobesberger, S.; Rantala, P.; et al. Direct observations of atmospheric aerosol nucleation. *Science* **2013**, *339*, 943–946. [[CrossRef](#)] [[PubMed](#)]

46. Krasnomowitz, J.M.; Apsokardu, M.J.; Stangl, C.M.; Tiszenkel, L.; Ouyang, Q.; Lee, S.; Johnston, M.V. Growth of Aitken mode ammonium sulfate particles by  $\alpha$ -pinene ozonolysis. *Aerosol Sci. Technol.* **2019**, *53*, 406–418. [[CrossRef](#)]
47. Ye, J.; Abbatt, J.P.D.; Chan, A.W.H. Novel pathway of SO<sub>2</sub> oxidation in the atmosphere: Reactions with monoterpene ozonolysis intermediates and secondary organic aerosol. *Atmos. Chem. Phys.* **2018**, *18*, 5549–5565. [[CrossRef](#)]
48. Jang, M.; Czoschke, N.M.; Lee, S.; Kamens, R.M. Heterogeneous atmospheric aerosol production by acid-catalyzed particle-phase reactions. *Science* **2002**, *298*, 814–817. [[CrossRef](#)]
49. Czoschke, N. Effect of acidic seed on biogenic secondary organic aerosol growth. *Atmos. Environ.* **2003**, *37*, 4287–4299. [[CrossRef](#)]
50. Nenes, A.; Pandis, S.N.; Pilinis, C. ISORROPIA: A new thermodynamic equilibrium model for multiphase multicomponent inorganic aerosols. *Aquat. Geochem.* **1998**, *4*, 123–152. [[CrossRef](#)]
51. Ng, N.L.; Canagaratna, M.R.; Jimenez, J.L.; Chhabra, P.S.; Seinfeld, J.H.; Worsnop, D.R. Changes in organic aerosol composition with aging inferred from aerosol mass spectra. *Atmos. Chem. Phys.* **2011**, *11*, 6465–6474. [[CrossRef](#)]
52. Zhu, M.; Jiang, B.; Li, S.; Yu, Q.; Yu, X.; Zhang, Y.; Bi, X.; Yu, J.; George, C.; Yu, Z.; et al. Organosulfur compounds formed from heterogeneous reaction between SO<sub>2</sub> and particulate-bound unsaturated fatty acids in ambient air. *Environ. Sci. Technol. Lett.* **2019**, *6*, 318–322. [[CrossRef](#)]
53. Zhu, M.; Wang, S.; Zhang, Y.; Yu, Z.; Yu, Y.; Wang, X. Particle-bound highly oxidized organic molecules derived from aromatic hydrocarbons in an urban atmosphere. *Environ. Sci. Technol. Lett.* **2022**, *9*, 1030–1036. [[CrossRef](#)]

**Disclaimer/Publisher's Note:** The statements, opinions and data contained in all publications are solely those of the individual author(s) and contributor(s) and not of MDPI and/or the editor(s). MDPI and/or the editor(s) disclaim responsibility for any injury to people or property resulting from any ideas, methods, instructions or products referred to in the content.